11-24-2022

Coupling Evidence From Lower Atmosphere to Mesosphere and Ionosphere Through Quasi 27-Day Oscillation

Alan Z. Liu
Embry-Riddle Aeronautical University, liuz2@erau.edu

Kaiming Huang
Wuhan University

Hao Cheng
Wuhan University

Shaodong Zhang
Wuhan University

Chunming Huang
Wuhan University

See next page for additional authors

Scholarly Commons Citation
Kaiming Huang, Hao Cheng, Alan Z Liu, et al. Coupling evidence from lower atmosphere to mesosphere and ionosphere through quasi 27-day oscillation. ESS Open Archive. September 24, 2019. DOI: https://doi.org/10.1002/essoar.10501034.1

Authors
Alan Z. Liu, Kaiming Huang, Hao Cheng, Shaodong Zhang, Chunming Huang, Yun Gong, and Gang Chen

Coupling evidence from lower atmosphere to mesosphere and ionosphere through quasi 27-day oscillation

Hao Cheng[1,2,3] Kai Ming Huang[1,3,4] Alan Z. Liu[5] Shao Dong Zhang[1,3] Chun Ming Huang[1,3] Yun Gong[1,3] and Gang Chen[1]

[1]School of Electronic Information, Wuhan University, Wuhan, China

[2]Key Laboratory of Geospace Environment, Chinese Academy of Sciences, University of Science and Technology of China, Hefei, China

[3] Key Laboratory of Geospace Environment and Geodesy, Ministry of Education, Wuhan, China

[4]State Observatory for Atmospheric Remote Sensing, Wuhan, China

[5]Department of Physical Science, Embry-Riddle Aeronautical University, Daytona Beach, Florida, USA

Email Address: hkm@whu.edu.cn

Zip code: 430072

Abstract. Using meteor radar, radiosonde and digisonde observations and MERRA-2 reanalysis data from 12 August to 31 October 2006, we report a dynamical coupling from the tropical lower atmosphere to the mesosphere and ionospheric F2 region through a quasi 27-day intraseasonal oscillation (ISO). It is interesting that the quasi 27-day ISO is active in the troposphere and stratopause and mesopause regions, exhibiting a three-layer structure. In the mesosphere and lower thermosphere (MLT), the amplitude in the zonal wind increases from about 4 ms^{-1} at 90 km to 15 ms^{-1} at 100 km, which is different from previous observations that ISOs generally have the amplitude peak at about 80-85 km, and then weakens with height. OLR and specific humidity data demonstrate that there is a quasi 27-day periodicity in convective activity in the tropics, which causes the ISO of the zonal wind and gravity wave (GW) activity in the troposphere. GW energy in the stratosphere also exhibits a sharp spectral speak at 27-day period, meaning that the convectively modulated GWs play a vital role in driving the oscillation in the MLT. The quasi 27-day variability arises clearly in the hmF2. Wavelet analysis shows that the dominant period and active time of the hmF2 oscillation are in good agreement with those in the zonal wind of the MLT and OLR rather than in the F10.7 and Kp index. Hence, tropical convective activity has an influence on the dynamics of the MLT and F2 region through modulated waves and ISOs.

1. Introduction

The circulation of the tropical stratosphere, mesosphere and lower thermosphere (MLT) is characterized by quasi-biennial (QBO), annual (AO), and semiannual (SAO) oscillations (Baldwin et al., 2001). In the tropics, convective activity is active due to intense solar radiation, which can excite planetary scale Kelvin and Rossby waves, and mid and small scale gravity waves (GWs). It is generally accepted that waves with different scales generated in the lower atmosphere play a vital role in driving

QBO and SAO at different heights through their upward propagation and interaction with the background flow (Lindzen, 1981; Dunkerton, 1997). Hence, oscillation and wave propagation and their intercoupling dominate the dynamical process in the tropical atmosphere.

Oscillation with seasonal time scale was noticed slightly later than the well-known QBO (Ebdon, 1960; Reed et al., 1961). Madden and Julian (1971, 1972) discovered a 40 to 50-day oscillation of the zonal wind in the tropical troposphere, which is referred to as the Madden-Julian oscillation (MJO). Afterwards, as the advancement of atmospheric sounding, more periodic oscillations were found in the tropical zonal wind and temperature, thus intraseasonal oscillation (ISO) is often extended to be quasi-periodic variations of about 20-100 days (Ghil & Mo, 1991; Eckermann et al., 1997; Isoda et al., 2004). A number of observations reveal that ISOs are a prominent variability in the tropical atmosphere (Madden, 1986; Gutzler & Madden, 1989; Ghil & Mo, 1991; Hendon & Salby, 1994; Eckermann et al., 1997; Lieberman, 1998; Kumar et al., 2007; Deshpande et al., 2011; Niranjankumar et al., 2011; Guharay et al., 2017; Li et al., 2018). Until now, ISOs have attracted extensive attention because of not only their complex dynamics but also their important influences on monsoons (Lawrence & Webster, 2001; Zhou & Chan, 2005; Karmakar & Krishnamurti, 2019), tropical cyclone (Huang et al., 2011; Yang et al., 2015), and cloud and precipitation (Benedict & Randall, 2007; Lau & Wu, 2010; Barnes & Houze Jr, 2013).

Theoretical, modeling and observational studies paid great efforts with regards to spatial structures, propagation patterns and generation mechanisms of ISOs. ISOs can propagate either eastward, showing Kelvin wave features, or westward, displaying Rossby wave characteristics, which is explained in terms of an equatorial convectively coupled Kelvin-Rossby couplet (Lau & Peng, 1990; Wang & Xie, 1996, 1997). Interactions between eastward propagating ISOs and mean flow can also generate an unstable Rossby wave with horizontal scale of thousands of kilometers (Lau & Peng, 1990). Easterly vertical shears (Jiang et al., 2004), air-sea interaction (Fu & Wang, 2004), eddy momentum transport from synoptic systems (Hsu & Li, 2011) could contribute to the northward propagation component of ISOs, and beta drift of synoptic motion may induce the northward propagation of ISOs (Boos & Kuang, 2010). Although tropical ISOs are mainly originated from convectively coupled wave dynamics involving Kelvin and Rossby waves through latent heat released in precipitation, atmospheric response to independent forcing, atmospheric instability, water vapor variation, nonlinear heating from sea surface temperature, multiscale interaction, and solar irradiance are proposed to be possible mechanisms of ISO generation (Madden & Julian, 1994; Zhang, 2005).

When ISO generated in the tropical lower atmosphere propagates upward, its amplitude often quickly decays above the tropopause (Madden & Julian, 1971; Rao et al., 2009; Guharay et al., 2014). However, some studies show that ISO may strengthen again in the upper stratosphere. Kumar and Jain (1994) proposed that ISO could propagate upward to the stratosphere from the tropical troposphere via leakage of its partial energy into the stratosphere. Ziemke and Stanford (1991) showed that strong ISO activity associated with tropical Rossby waves in the lower atmosphere of the Southern Hemisphere (SH) could propagate to the upper stratosphere by refracting out to mid latitudes and then refracting back to the equatorial stratospause region, and similar phenomenon in the Northern Hemisphere (NH) was inferred based on rocketsonde and radiosonde observations (Nagpal et al., 1994). Niranjankumar et al. (2011) suggested that partial refraction and reflection in the troposphere are related with subtropical jet when investigating vertical and lateral propagation features of ISO. Numerical investigation demonstrated that Rossby waves forced by the induced heating on the equator could radiate poleward into the extratropical westerlies and vertically into the stratosphere in the two hemispheres (Salby et al., 1994).

In the MLT, ISOs with a wide period range of 20-60 days were reported in the zonal wind over

Christmas Island (2°N, 157°W) based on medium frequency (MF) radar observation (Eckermann & Vincent, 1994). The study indicated that it is unlikely that the ISOs propagate up to the MLT from the lower atmosphere although they were supposed to originate from in the lower atmosphere. A further investigation by Eckermann et al. (1997) found that ISO patterns in the MLT occur not only in zonal wind but also in GW variances and diurnal tidal amplitudes, thus they suggested that GWs and tides modulated by ISOs in tropical convection could induce in turn similar periodicities in the zonal flow of the MLT by transferring their momentum and energy into the mean flow as these waves propagate up to the MLT. By analyzing the correlations between ISO of the zonal wind and wave amplitudes in the equatorial MLT form three radar observations, Isoda et al. (2004) argued that nonmigrating tides are modulated at ISO period in the lower atmosphere, and by propagating to the MLT, the breaking and dissipating tides drive the variation of the zonal mean wind, but the contribution of GWs to the ISO in the MLT is unclear. There is a consistency of ISOs between convective activity in the lower atmosphere and the zonal wind in the MLT based on MF and meteor radar observations at low latitudes, implying similar ISO of the zonal wind in the MLT driven by modulated wave forcing (Kumar et al., 2007; Rao et al., 2009). Lower stratospheric GW potential energy derived from Constellation Observing System for Meteorology, Ionosphere, and Climate (COSMIC) radio occultation satellite measurement shows a strong correlation with the tropospheric zonal winds due to filtering of upward propagating GWs by the MJO wind (Moss et al., 2016). Middle stratospheric GW temperature variances observed by Atmospheric Infrared Sounder (AIRS) display an intraseasonal variability because the zonal wind around the tropopause likely controls GW propagation into the stratosphere by a critical level filtering, meaning that MJO can modulate the middle atmospheric circulation through regulating GWs by means of generation and propagation (Tsuchiya et al., 2016). However, using meteor radar data at mid and high latitudes, Pancheva et al. (2003) noticed an obvious ISO in the MLT, but there was not a corresponding periodicity in atmospheric wave activities, including GWs, tides and quasi 2-day PWs. In addition, Huang et al. (2015) presented that an ISO with relatively short period of 27 days could penetrate tropopause region and weak westward wind field in the lower stratosphere to propagate upward into the MLT, while an ISO with long period of about 46 days does not so.

Quasi 27-day ISO arouses attention because this variability has the same period as solar rotation. Quasi 27-day periodicity is often observed in the zonal wind, temperature, and trace gases at different heights from the troposphere to the MLT (Fioletov, 2009; Huang et al., 2015; Hood, 2016; Guharay et al., 2017; Thiéblemont et al., 2018). Although trace gases have a clear response to solar 27-day cycle, the attribution of 27-day periodicity in the atmosphere to a solar cause is complicated by the fact that internal variability of the atmosphere can itself also generate quasi 27-day oscillation (Hoffmann & von Savigny, 2019). Both chemistry-climate model (CCM) and whole atmosphere community climate model (WACCM) results show that a 27-day variability in the wind and temperature is an inherent feature of the atmosphere, thus is not necessarily related to the solar rotational period since CCM and WACCM can output quasi 27-day variation even without solar rotational forcing (Schanz et al., 2016; Sukhodolov et al., 2017). Similar to the response of ozone in the upper stratosphere to solar rotation through physicochemical mechanisms, the presence of quasi 27-day oscillation in the ionospheric variability is a natural event as solar radiation is a major source of energy and ionization. The effects of solar rotation on ionospheric key parameters, such as total electron content (TEC), peak electron density of F2 layer (NmF2), maximum height of F2 layer (hmF2), and critical frequency of F2 layer (foF2), are extensively investigated by observational and modeling studies (Pancheva et al., 1991; Rich et al., 2003; Min et al., 2009; Xu et al., 2011; Coley & Heelis, 2012; Ma et al., 2012; Ren et al., 2018).

Nevertheless, many investigations show that long-period solar flux changes of 11-year solar cycle are the major source of ionospheric variability, and compared to long-term solar changes, 27-day solar rotation and annual and semiannual variations associated solar zenith angle represent small variability (Forbes et al., 2000; Richards, 2001; Liu et al., 2006; Solomon et al., 2018). The ionospheric variability with periods between 2 and 30 days is mainly caused by geomagnetic activity and equally important "meteorological influences" transmitted from lower levels (Forbes et al., 2000, 2018; Rishbeth & Mendillo, 2001; Laštovička, 2006; Borries & Hoffmann, 2010). Mikhailov et al. (2004) analyzed ionospheric F2-layer disturbances not related to geomagnetic activity based on records over 26 ionosonde stations. Ionospheric disturbances in quiet time of the Sun are not only rather frequent but their amplitude is comparable to the amplitude of moderate F2-layer storm effects, and these perturbations may partly be attributed to the impact from below. By using hmF2 data from digisonde measurement at Millstone Hill, Pancheva et al. (2002) demonstrated that the 27-day oscillations in hmF2 are generated by geomagnetic activity and by 27-day oscillation present in the zonal neutral wind of the MLT. Hence, the dynamics in the MLT play a significant role in ionospheric variability.

In this work, a quasi 27-day ISO activity in the tropics is reported. The oscillation exhibits a characteristic variation with height in the MLT, being different from previous observations, and leads to a corresponding change in the ionosphere. We attempt to reveal its generation in the lower atmosphere and the coupling from the troposphere to the ionosphere through this oscillation. Section 2 covers a brief explanation of the data that we utilized. In section 3, we provide the quasi 27-day variability throughout the troposphere to the thermosphere. Section 4 discuss the origination of the oscillation in different atmospheric layers, and a summary is presented in Section 5.

2. Data

2.1 Meteor Radar Observation

The horizontal wind from a meteor radar located in Kihei on Maui, Hawaii, at 20.75°N, 156°W, is used in the study. The radar system is an all-sky interferometric meteor (SKiYMET) radar with an operating frequency of 40.92 MHz, which adopts a 3-element Yagi antenna pointing zenith to illuminate meteor trails. Five 3-element Yagi antennas oriented along two orthogonal baselines are used to receive echoes from the meteor trails. The hourly horizontal wind at 1 km height interval in the height range of 80-100 km is estimated based on meteor trail position and Doppler shift. A technical description of SKiYMET radar can be found in the work of Hocking et al. (2001). The Maui meteor radar system and the wind computation are described in detail by Franke et al. (2005). The meteor radar observation has been applied to exploring dynamical processes in the MLT over Maui (Lu et al., 2011; Liu at., 2013; Huang et al., 2013a, 2013b).

In the paper, the horizontal wind data for 81 days from 12 August to 31 October 2006 is utilized. In this period of our attention, the missing data decreases to a minimum value of 1.3% at 90 km from about 12.9% at 80 km and 15.6% at 100 km, thus the highly effective observation is suitable for the investigation of the atmospheric oscillation in the MLT region.

2.2 Digisonde Observation

We use the hmF2 to examine the ionospheric response to the atmospheric oscillation. The hmF2 data is obtained from the digital ionosonde database (DIDBase) of University of Massachusetts Lowell (Galkin et al., 1999; Reinisch et al., 2004), which is accessed from the website at http://www.digisonde.com. The hmF2 is observed from the DPS-4 digisonde installed in Kwajalein Island (9.4°N, 167.4°E), with a temporal resolution of 5 min.

2.3 Radiosonde Observation

The United States radiosonde observations at three tropical stations distributed in the NH and SH are applied to the analysis of the oscillation activity in the troposphere and lower stratosphere. The data are archived and provided freely by the National Climatic Data Center (NCDC) of National Oceanic and

Atmospheric Administration (NOAA) through the Stratospheric Processes and Their Role in Climate (SPARC) Data Center at ftp://ftp.ncdc.noaa.gov. The three stations are situated at Hilo (19.72°N, 155.07°W), Kauai (21.98°N, 159.35°W) on Hawaii, and at Pago Pago (14.33°S, 170.72°W) on Samoa. Observational sites are sparse in the Pacific, thus we choose the radiosonde and digisonde stations as close as possible to the meteor radar station.

Routine radiosondes are usually launched twice daily at 00:00 and 12:00 UT. As a balloon rises, atmospheric horizontal wind, temperature, pressure, and relative humidity are sensed by balloon-borne platform. The sampled heights depend on ascent rate of balloon, ranging from 10 to 100 m. For convenience, we interpolate the raw data linearly to a uniform interval of 50 m. The maximum height of a radiosonde observation is its balloon burst altitude. In the period that we focus on, about 90%, 88% and 90% of balloons reached 30 km in Hilo, Kauai and Pago Pago, respectively, but only about 63%, 87% and 87% attained 31 km. Hence, we select the altitude of 30 km as the upper height limit of radiosonde observation in our analysis.

We follow the method proposed by Alduchov and Eskridge (1996) to derive specific humidity from temperature, pressure and relative humidity measured by radiosonde.

2.4 Outgoing Longwave Radiation

Specific humidity and outgoing longwave radiation (OLR) have often been used as proxies of convective activity over the tropical region (Arkin & Ardanuy, 1989). We expect to explore the origin of the tropical oscillation by combining specific humidity and OLR. Daily OLR data is obtained from the NOAA at the Website of https://www.esrl.noaa.gov/psd, with a 2.5° latitudinal and longitudinal resolution (Liebmanna & Smith, 1996).

2.5 Solar and Geomagnetic indices

We also examined solar and geomagnetic forcing as potential controlling factors of the atmosphere.

Daily solar 10.7 cm radio flux (F10.7) and 3-h Kp index data provided from the National Centers for Environmental Information (NCEI) of NOAA at the Website of https://www.ngdc.noaa.gov are used as measures of solar and geomagnetic activities. The measurements were taken during the late declining phase of solar cycle 23.

2.6 Reanalysis Data

The Modern-Era Retrospective Analysis for Research and Applications (MERRA) reanalysis of the National Aeronautics and Space Administration (NASA) is an ideal candidate to examine the features of the oscillation in the zonal, meridional and vertical directions. The product of "inst6_3d_ana_Nv" in the version 2 of MERRA (MERRA-2) is available through the NASA Goddard Earth Sciences Data and Information Services Center (GES DISC) online archive at https://disc.gsfc.nasa.gov/datasets. The reanalysis data is 6-hourly instantaneous analysis fields on a 0.5°× 0.625° latitude-by-longitude grid at 72 model levels from ground up to 0.01 hPa (Gelaro et al., 2017).

All the data used in the present study are in the same period from 12 August to 31 October 2006, and 12 November 2006 is referred to as day 1.

3. Quasi 27-Day Oscillation

3.1 Oscillation in MLT

Figure 1 shows the daily averaged zonal and meridional winds measured by the meteor radar for 81 days from 12 August to 31 October 2006. The mean zonal wind (positive eastward) has a maximum of 50.7 ms^{-1} at 95 km on day 59 and a minimum of -67.0 ms^{-1} at 100 km on day 24, while the mean meridional wind (positive northward) is between -59.3 and 40.0 ms^{-1}. The different temporal scales of the perturbations can be noted in the wind field.

We carry out a Lomb-Scargle spectrum analysis (Scargle, 1982), with a 4-times oversampling, on the daily averaged zonal and meridional winds to investigate their spectral components. Figure 2 shows the Lomb-Scargle spectral of the mean zonal and meridional winds. A confidence level of 95% corresponds to a spectral amplitude of 7.4 ms^{-1}. It is interesting that the spectral components in the zonal wind are very weak blow 90 km, while above 90 km, a quasi 27-day oscillation is a predominant component, and strengthens gradually with height. Its spectral amplitude grows to 15.2 ms^{-1} at 100 km from 4.2 ms^{-1} at 90 km. Based on over five years of wind data acquired by a MF radar at Christmas Island, Eckermann et al. (1997) showed that the ~60-day ISO in the zonal wind of the MLT is relatively strong in winter-early spring (December-April). Its amplitude reaches a peak of about 10-15 ms^{-1} at 80-85 km, and then clearly decreases with height. Similarly, by using a 20-year radar observation at four sites from 70°N to 30°N, the investigation indicated that the oscillation in the zonal wind with period between 20 and 40 days at mid and high latitudes is active in winter (November-March), with a strength reduction from about 10 ms^{-1} at 75-85 km to about 5 ms^{-1} near 100 km (Luo et al., 2001). Huang et al. (2015) presented a quasi 27-day oscillation event in December 2004 to March 2005 over Maui with large amplitudes throughout the MLT. Its amplitude has a maximum value of 20.3 ms^{-1} in the zonal wind at 89 km, and then monotonously drops to 7.5 ms^{-1} at 96 km. Hence, in the paper, we note that a relatively intense quasi 27-day oscillation occurs in August-October, and its evolution with height in the MLT is different from those in the previous studies (Eckermann et al., 1997; Luo et al., 2001; Huang et al., 2015). The quasi 27-day periodicity also arises in the meridional wind and shows a similar vertical variation but with a weak spectral magnitude. This is consistent with early observations that atmospheric oscillation occurs mainly in the zonal wind (Eckermann et al., 1997; Luo et al., 2001; Huang et al., 2015), thus we will concentrate on the zonal wind oscillation.

In order to determine the vertical propagation of the oscillation, a sinusoidal wave fitting under a 27-day period is applied to the time series of the mean zonal wind at 90-100 km. The fitted amplitude and phase are shown in Figure 3. Here, the phase is described by the time when the oscillation attains its maximum value (Huang et al., 2015). It can be seen from Figure 3 that the amplitude of the oscillation gradually increases from 4.3 ms^{-1} at 90 km to 15.2 ms^{-1} at 100 km, which is in good agreement with the spectral result in Figure 2. A linear fitting of the phase exhibits a slow downward phase progression in the MLT.

3.2 Oscillation in Ionosphere

It is generally recognized that the 27-day periodicity in the ionosphere can originate from the effects of the solar rotation, geomagnetic activity and zonal neutral wind in the MLT (Pancheva et al., 2002; Liu et al., 2006; Borries & Hoffmann, 2010; Ma et al., 2012). Here, we use the hmF2 data over the tropical Kwajalein Island to examine its variation during this time. A wavelet transform is performed on the hourly mean hmF2 time series. Morlet wavelet function which consists of a plane wave modulated by a Gaussian envelope is chosen as mother wavelet. Wavelet analysis decomposes a time series into a two-dimensional time-frequency domain, thus it can provide not only the dominant components but also the variation of these components with time.

Figure 4 shows the wavelet spectrum of the hourly mean hmF2 from 12 August to 31 October 2006. The perturbation periods are limited to 15-45 days to highlight the quasi 27-day periodicity. For comparison, the wavelet transform for the linearly interpolated zonal wind at 100 km above Maui is also presented in Figure 4. Figure 4 illustrates that the quasi 27-day oscillation takes place in the hmF2, and the onset of the hmF2 oscillation legs behind the oscillation in the zonal wind at 100 km. Similarly, Pancheva et al. (2002) found that the quasi 27-day variation in the hmF2 above Millstone Hill can be generated by the quasi 27-day oscillation in the zonal neutral wind of the MLT but with 5-6 day delay. Some observational and modeling studies indicated that most GWs and tides could propagate into the ionosphere directly from the MLT, and oscillations at periods of 2-30 days might propagate upward to the F-region indirectly via the potential mechanism of modulation by upward propagating tides (Laštovička, 2006; Pancheva et al., 2006; Borries & Hoffmann, 2010; Forbes et al., 2018). Hence, the quasi 27-day oscillation can lead to the dynamical and electrodynamical coupling between the MLT and the F2-region in this indirect way.

3.3 Oscillation in Troposphere and Stratosphere

We use the radiosonde observations and MERRA-2 reanalysis data to examine the activity of the quasi 27-day oscillation in the troposphere and stratosphere. Figure 5 presents the Lomb-Scargle spectrum of the zonal wind measured by the radiosonde in Hilo and Kauai on Hawaii close to the Maui meteor radar. The spectral analysis in Figure 5 illustrates that the quasi 27-day periodicity appears clearly below about 17 km with a maximum magnitude of about 7 ms^{-1} around 13 km. However, it does not have a significant spectral peak above 17 km where the tropopause is, indicating that it is difficult for the oscillation to penetrate through the tropopause region into the lower stratosphere. This is in agreement with rapid attenuation of ISOs above the tropopause presented in many early observations (Madden & Julian, 1971; Ziemke & Stanford, 1991; Rao et al., 2009; Niranjankumar et al., 2011; Guharay et al., 2014).

In order to extend zonal wind information to higher altitudes, Figure 6 plots the Lomb-Scargle spectrum of the zonal wind above Maui from the MERRA-2 reanalysis. The right vertical axis marks the approximate heights of the pressure levels derived from logarithmic pressure-height formula. The spectral feature below 10 hPa (~32 km) in the reanalysis data is roughly consistent with that in the radiosonde observations. A quasi 27-day periodicity occurs below 108.7 hPa (~16 km) level with an intensity similar to the radiosonde measurements in Hilo and Kauai. It is interesting that the quasi 27-day oscillation evidently appears between 3.3 and 3.27×10^{-2} hPa (~40-72 km) levels with a spectral peak of 11.2 ms^{-1} at 0.48 hPa (~53 km) level, and has a narrower spectral width than in the lower atmosphere. However, there is not a significant spectral component of quasi 27-day period at 3.27×10^{-2}-1.0×10^{-2} (~72-80 km) levels, close to the lowest altitude of 80 km in the meteor radar observation. Based on the radar observation, this oscillation is markedly strengthened above 90 km again, as shown in Figure 2. Hence, the quasi 27-day oscillation exhibits a three-layer structure from the troposphere to the MLT over Maui.

To examine the meridional feature of the quasi 27-day oscillation, we make a sinusoidal wave fitting with a 27-day period on the zonal wind at 176.93 and 0.48 hPa (~12 and 53 km) levels along the 156.25°W longitude based on the MERRA-2 reanalysis data for a same duration of 81 days. The two pressure levels are chosen because the quasi 27-day component at these levels is strong, as shown in Figure 6. Figure 7 depicts the evolutions of the fitted amplitude and phase with latitude. The phase varies slowly with latitude, which seems to show a tendency of the oscillation propagation from the SH to the NH. The amplitudes have several extreme values between 25°S and 25°N, especially the maximal values around 20°S and 20°N at 176.93 hPa. In that case, we present the Lomb-Scargle spectrum of the zonal wind from the radiosonde observation in Pago Pago of the SH, which is shown in Figure 5(c). It can be noted that the quasi 27-day oscillation in the troposphere is more prominent above Pago Pago than above Hilo and Kauai. Therefore, the oscillation is active at low latitudes in the both hemispheres.

4. Discussion

As shown in Figures 5 and 6, the quasi 27-day oscillation can be identified in the troposphere, but does not appear clearly in the lower stratosphere. Eckermann and Vincent (1994) reported the ISOs with periods of 35-60 days in the zonal wind in the equatorial MLT based on MF radar observation, and argued that it is unlikely for these ISOs to propagate to the MLT from the lower atmosphere. Instead, they proposed that GWs and tides generated by tropical convection are modulated by the oscillations in the lower atmosphere and then in turn drive similar periodicities in the MLT when propagating to the MLT and depositing their energy and momentum into the mean flow through instability (Eckermann & Vincent, 1994; Eckermann et al., 1997). According to this mechanism of wave coupling among the different atmospheric layer, we investigate the GW activity in the lower atmosphere based on the radiosonde observations in the tropic Hilo, Kauai and Pago Pago. The GW perturbations are analyzed separately at 1-9 km of the troposphere and at 20-28 km of the lower stratosphere, which is for three reasons: 1) avoiding the sharp variations of the zonal wind and temperature from the upper troposphere to the lower stratosphere; 2) the approximately constant buoyancy frequency in each chosen height ranges; and 3) examining the GW features in the convective source region of 1-9 km and in the propagation region of 20-28 km.

We follow the analysis technique of Allen and Vincent (1995) and Vincent and Alexander (2000) to derive the GW perturbations from the profiles of radiosonde sounding. Assuming that the observed zonal wind, meridional wind and temperature $[u, v, T]$ mainly consist of the background $[\overline{u}, \overline{v}, \overline{T}]$ and GW perturbations $[u', v', T']$, we estimate the background $[\overline{u}, \overline{v}, \overline{T}]$ by fitting a second-order polynomial to the vertical profiles of $[u, v, T]$ in the chosen height interval. This second-order polynomial fitted background was widely used in GW analysis from radiosonde observations (Allen & Vincent, 1995; Vincent & Alexander 2000; Zhang & Yi, 2007; Huang et al., 2018), which can reduce the effect of long vertical wavelength waves. The total fluctuation quantities are obtained from the observed profiles by removing the fitted second-order polynomial. In order to remove fluctuations due to smaller-scale effects, such as measurement error, drag variation of balloon, noise introduced by the interpolation process (Zhang et al, 2012), we apply a high-pass filter to extract the GW components from the total fluctuation. The cutoff wavelength of the filter is selected to be 0.5 km since extensive observations show the GW vertical wavelengths are in general more than 0.5 km. The total energy per unit mass (E) is used as a measurement for GW activity, which is written as follows (Allen & Vincent, 1995; Vincent & Alexander 2000),

$$E=\frac{1}{2}\left[\overline{u'^2}+\overline{v'^2}+\frac{g^2\overline{\widehat{T'}^2}}{N^2}\right] \tag{1}$$

where $\widehat{T'}=\frac{T'}{\overline{T}}$ is the normalized temperature perturbation; g is the acceleration due to gravity; N is the buoyancy frequency; and the overbar means an unweighted average over height. The vertical wind perturbation of GWs is neglected in Eq. (1) because there is no vertical wind in radiosonde observation, and the vertical wind perturbation of GWs is much smaller than their horizontal wind perturbation.

We derive the total energy of GWs from the observed profiles of radiosonde in Hilo, Kauai and Pago Pago, and then calculate the daily averaged energy in Pago Pago of the SH and between the two station of the NH, respectively, for the sake of reducing the impact of chance events. Figure 8 shows the Lomb-Scargle spectra of daily mean GW energies at 1-9 km of the troposphere and 20-28 km of the lower stratosphere in the NH and SH. One can note from Figure 8 that a quasi 27-day oscillation of GW energy occurs in both the troposphere and the lower stratosphere. The quasi 27-day periodicity has a stronger spectral intensity in the lower stratosphere than in the troposphere because the GW amplitude increases with height owing to the exponentially decreasing atmospheric density. Importantly, although the quasi 27-day oscillation does not evidently appear in the lower stratospheric wind field, its spectral peak in the GW energy is much sharper in the lower stratosphere than in the troposphere, which may be due to the filtering effect by the quasi 27-day variation in the tropospheric wind field (Moss et al., 2016; Tsuchiya et al., 2016), as shown in Figure 5. Therefore, the GW energy investigation seems to support the coupling mechanism that GWs modulated by oscillation in the lower atmosphere induce the similar periodicity in the MLT through their energy and momentum transport (Eckermann & Vincent, 1994; Eckermann et al., 1997).

As for the ISO enhancement in the upper stratosphere again, there are two possible mechanisms proposed in previous studies. Kumar and Jain (1994) argued that ISO propagates directly upward to the stratosphere from the tropical troposphere through partial energy transmission, and Huang et al. (2015) confirmed the ISO penetration into the stratosphere based on the radiosonde observation. Ziemke and Stanford (1991) suggested that upward propagating ISO is refracted to mid latitudes, and then refracted back into the tropical upper stratosphere. The phase in the stratosphere shown in Figure 7(a) seems to imply that the oscillation propagates towards the NH low latitudes from the NH and SH mid latitudes. In addition, the quasi 27-day oscillation may be partially attributable to GWs. As the GWs modulated at a 27-day period propagate to the upper stratosphere, they may deposit their partial momentum and energy into the background flow by means of instability and background wind filtering. The GWs with their remaining energy can further propagate to higher levels and further induce the quasi 27-day variability in the mesopause region. Still, the contribution of tidal waves cannot be ruled out since we cannot examine the tidal activity in the lower atmosphere due to a coarse temporal resolution of 12 h in the radiosonde measurement.

Earlier studies discussed possible mechanisms of ISO generation (Zhang, 2005). It is generally recognized that ISOs in the tropics originate mainly from convective activity. OLR is often used as a proxy of convection activity. We choose the OLR data at the locations of (20°N, 157.5°W) and (15°S, 170°W), close to Maui and Pago Pago, to examine the convective activity, and then carry out a wavelet transform on the OLR. Figure 9 presents their wavelet spectra. It shows that there is a quasi 27-day variation in the OLR over the two tropical sites. We also calculate the specific humidity from the radiosonde observation in Pago Pago. Figure 10 shows the Lomb-Scargle spectrum of the specific humidity from the radiosonde measurement and the reanalysis data above Pago Pago. The spectra of specific humidity between the observation and reanalysis data are consistent with each other. The quasi

27-day periodicity is the dominant component in the water vapor variation, and the spectral analysis above 7 km (not presented here) indicates that the dominant 27-day component extends all the way to the tropopause region. Hence, the periodicity in the OLR and water vapor demonstrates that there is a quasi 27-day variability in the convective activity in the tropics. Since convections are a main source of tropical waves and ISOs (Fritts & Alexander, 2003; Zhang, 2005), their variability can lead to the quasi 27-day ISO not only in the zonal wind but also in the GW activity in the tropical troposphere. When the GWs generated in the convection source region propagate upward, they are further modulated by the quasi 27-day oscillation of the zonal wind, resulting in a more prominent 27-day periodicity of the GW activity in the stratosphere than in the troposphere, as shown in Figure 8.

The ionospheric activity is complex because it is affected not only by solar and geomagnetic activities, but also by neutral-plasma interaction, thus the oscillation in the hmF2 may have several possible origins (Forbes et al., 2000; Pancheva et al., 2002). We investigate the relationship of the hmF2 oscillation with solar radiation and geomagnetic activity to reveal its main origin. Here, F10.7 and Kp index are chosen as proxies for solar radiation and geomagnetic activity, respectively. Figure 11 depicts that the wavelet spectra of the F10.7 and Kp index in the duration of our attention. One can see from Figure 11 that the F10.7 has an oscillation with a dominant period less than 27 days. The F10.7 oscillation is weak because the year 2006 is in the late declining phase of solar cycle 23, and the weak oscillation arises mainly before day 40. The geomagnetic activity exhibits a significant quasi 27-day variation between about day 10 and 36. The hmF2 oscillation shown in Figure 4(a) is robust after about day 30. By comparing Figure 4(a) with Figures 4(b), 9 and 11, it can clearly be noted that both the dominant period and active time of the hmF2 oscillation are in better correlation with the variabilities in the wind field and OLR rather than in the F10.7 and geomagnetic activity. Hence, the hmF2 periodicity originates mainly from the oscillation in the convection, waves and wind field, which demonstrates that the quasi 27-day variability in the ionosphere can also come from the natural wind and "meteorological influences" from below (Forbes et al., 2000; Pancheva et al., 2002). In other words, the variability in the tropical convective activity drives the ISO in the zonal wind and modulates the wave activity in the lower atmosphere, which leads to a coupling from the lower atmosphere to the MLT and F2 region through wave propagation and wave-flow interactions (Forbes et al., 2000, 2018).

5 Summary

Combining the meteor radar, radiosonde and digisonde observations and the MERRA-2 reanalysis data for 81days from 12 August to 31 October 2006, we study a quasi 27-day ISO event in the tropical zonal wind from the troposphere to MLT, and the corresponding hmF2 variability generated from the oscillation.

The radiosonde observations at the three tropical stations distributed in the NH and SH show that the quasi 27-day oscillation originates from the lower atmosphere, and has an amplitude of about 7 ms^{-1} in the zonal wind in the upper troposphere. Above the tropopause, the oscillation attenuates rapidly, which is in agreement with most previous observations. The reanalysis data indicates that the quasi 27-day oscillation is strengthened in the upper stratosphere, and attains a magnitude of about 11 ms^{-1}. The ISO enhancement in the stratopause region is also reported in early studies. Whereas, the oscillation decays quickly again from about 70 km. The meteor radar measurement illustrates that the oscillation increases again from about 90 km, and reaches an intensity of about 15 ms^{-1} at 100 km. Hence, the quasi 27-day oscillation exhibits an interesting three-layer structure from the troposphere to the MLT. The oscillation in the MLT is different from the previous observations in which the ISO in the zonal wind generally has the amplitude peak at about 80-85 km, and then decreases with height (Eckermann et al., 1997; Luo et al., 2001; Huang et al., 2015). In the period that we focus on, the digisonde observation shows that the quasi 27-day variability arises clearly in the hmF2. This implies that a coupling from the lower atmosphere to the MLT and F2 region occurs through the quasi 27-day oscillation.

As proxies of convection activity, the OLR and specific humidity observations demonstrate that there is a quasi 27-day periodicity in the convective activity in the tropics. The convection is a main excitation source of tropical ISOs and waves, thus the quasi 27-day variability takes place not only in the zonal wind in the troposphere but also in the convectively modulated GW activity. As the GWs propagate upward, they can be modulated by the zonal wind oscillation in the upper troposphere. Hence, the quasi 27-day variability in the GW activity has a sharper spectrum in the lower stratosphere relative to that in the troposphere, even though the zonal wind in the lower stratosphere does not display a quasi 27-day ISO. The GWs may deposit their partial energy and momentum into the background flow in the stratopause region through the instability and background wind filtering, which might contribute partly to driving the quasi 27-day variability there, despite that the quasi 27-day ISO may be refracted back to the tropical stratopause region from midlatitudes. After partial energy loss, the GWs can further propagate upward to higher altitudes and induce the quasi 27-day ISO in the mesopause region through their momentum and energy deposition. Therefore, GWs play an important role in the connection of the quasi 27-day oscillation between the lower atmosphere and the MLT, as proposed by Eckermann and Vincent (1994) and Eckermann et al. (1997).

The 27-day variability in the ionosphere could originate from the periodicity of solar rotation, geomagnetic activity and zonal neutral wind or meteorological influences from below. The wavelet spectra of the F10.7 and Kp index indicate that in the time period we studied, the effects of solar rotation and geomagnetic activity are weak, and their quasi 27-day period arises before day 40. The hmF2 oscillation is robust after day 30, and its dominant period and active duration are in good agreement with those in the wind field of the MLT and OLR rather than in the F10.7 and Kp index. This demonstrates that the hmF2 periodicity originates mainly from the oscillation in the wind field associated with the convective activity. Therefore, the tropical convective activity can influence the dynamics of the MLT and F2 region through the propagation and interaction of these convectively modulated waves and ISOs.

Acknowledgments. We thank the NOAA for providing the radiosonde data at ftp://ftp.ncdc.noaa.gov, the OLR data at https://www.esrl.noaa.gov/psd and the F10.7 and Kp index data at https://www.ngdc.noaa.gov; University of Massachusetts Lowell for providing the hmF2 data at http://www.digisonde.com; and the NASA for providing the MERRA-2 data at https://disc.gsfc.nasa.gov/datasets. This work was jointly supported by the National Natural Science Foundation of China (through grants 41674151, 41974176, and 41531070), and the Open Program of Key Laboratory of Geospace Environment, CAS.

References

Alduchov, O. A., & Eskridge, R. E. (1996). Improved Magnus form approximation of saturation vapor pressure. *Journal of Applied Meteorology*, *35*, 601-609. https://doi.org/10.1175/1520-0450(1996)035<0601:IMFAOS>2.0.CO;2

Allen, S. J., & Vincent, R. A. (1995). Gravity wave activity in the lower atmosphere: Seasonal and latitudinal variations. *Journal of Geophysical Research: Atmospheres*, *100*, 1327-1350. https://doi.org/10.1029/94JD02688

Arkin, P. A., & Ardanuy, P. E. (1989). Estimating climatic-scale precipitation from space: A review. *Journal of Climate*, *2*, 1229-1238.

https://doi.org/10.1175/1520-0442(1989)002<1229:ECSPFS>2.0.CO;2

Baldwin, M. P., Gray, L. J., Dunkerton, T. J., Hamilton, K., Haynes, P. H., Randel, W. J., et al. (2001). The quasi-biennial oscillation. *Reviews of Geophysics*, *39*(2), 179-229. https://doi.org/10.1029/1999RG000073

Barnes, H. C., & Houze Jr, R. A. (2013). The precipitating cloud population of the Madden-Julian Oscillation over the Indian and west Pacific Oceans. *Journal of Geophysical Research: Atmospheres*, *118*, 6996-7023. https://doi.org/10.1002/jgrd.50375

Benedict, J. J., & Randall, D. A. (2007). Observed characteristics of the MJO relative to maximum rainfall. *Journal of the Atmospheric Sciences*, *64*, 2332-2354. https://doi.org/10.1175/JAS3968.1

Boos, W. R., & Kuang, Z. (2010). Mechanisms of poleward propagating, intraseasonal convective anomalies in cloud system-resolving models. *Journal of the Atmospheric Sciences*, *67*, 3673-3691. https://doi.org/10.1175/2010JAS3515.1

Borries, C., & Hoffmann, P. (2010). Characteristics of F2-layer planetary wave-type oscillations in northern middle and high latitudes during 2002 to 2008. *Journal of Geophysical Research: Space Physics*, *115*, A00G10. https://doi.org/10.1029/2010JA015456

Coley, W. R., & Heelis, R. A. (2012). Response of the equatorial topside ionosphere to 27-day variations in solar EUV input during a low solar activity period using C/NOFS. *Journal of Geophysical Research: Space Physics*, *117*, A03330. https://doi.org/10.1029/2011JA017301

Deshpande, S. M., Raj, P. E., & Konwar, M. (2011). Vertical variation of low-frequency oscillations in UHF radar derived winds at a tropical Indian station. *Journal of Geophysical Research: Atmospheres*, *116*, D24125. https://doi.org/10.1029/2011JD016226

Dunkerton, T. J. (1997). The role of gravity waves in the quasi-biennial oscillation. *Journal of Geophysical Research: Atmospheres*, *102*, 26053-26076. https://doi.org/10.1029/96JD02999

Ebdon, R.A. (1960). Notes on the wind flow at 50 mb in tropical and sub-tropical regions in January 1957 and January 1958. *Quarterly Journal of the Royal Meteorological Society*, *86*(370), 540-542. https://doi.org/10.1002/qj.49708637011

Eckermann, S. D., Rajopadhyaya, D. K., & Vincent, R. A. (1997). Intraseasonal wind variability in the equatorial mesosphere and lower thermosphere: long-term observations from the central Pacific. *Journal of Atmospheric and Solar-Terrestrial Physics*, *59*, 603-627. https://doi.org/10.1016/S1364-6826(96)00143-5

Eckermann, S. D., & Vincent, R. A. (1994). First observations of intraseasonal oscillations in the equatorial mesosphere and lower thermosphere. *Geophysical Research Letters*, *21*, 265-268. https://doi.org/10.1029/93GL02835

Fioletov, V. E. (2009). Estimating the 27-day and 11-year solar cycle variations in tropical upper stratospheric ozone. *Journal of Geophysical Research: Atmospheres*, *114*, D02302. https://doi.org/10.1029/2008JD010499

Forbes, J. M., Maute, A., Zhang, X., & Hagan, M. E. (2018). Oscillation of the ionosphere at planetary-wave periods. *Journal of Geophysical Research: Space Physics*, *123*, 7634-7649. https://doi.org/10.1029/2018JA025720

Forbes, J. M., Palo, S. E., & Zhang, X. (2000). Variability of the ionosphere. *Journal of Atmospheric and Solar-Terrestrial Physics*, *62*, 685-693. https://doi.org/10.1016/S1364-6826(00)00029-8

Franke, S. J., Chu, X., Liu, A. Z., & Hocking, W. K. (2005). Comparison of meteor radar and Na Doppler lidar measurements of winds in the mesopause region above Maui, Hawaii. *Journal of Geophysical Research: Atmospheres*, *110*, D09S02. https://doi.org/10.1029/2003JD004486

Fritts, D. C., & Alexander, M. J. (2003). Gravity wave dynamics and effects in the middle atmosphere. *Reviews of Geophysics*, *41*(1), 1003. https://doi.org/10.1029/2001RG000106

Fu, X., & Wang, B. (2004). Differences of boreal summer intraseasonal oscillations simulated in an atmosphere–ocean coupled model and an atmosphere-only model. *Journal of Climate*, *17*, 1263-1271. https://doi.org/10.1175/1520-0442(2004)017<1263:DOBSIO>2.0.CO;2

Galkin, I. A., Kitrosser, D. F., Kecic, Z., & Reinisch, B. W. (1999). Internet access to ionosondes. *Journal of Atmospheric and Solar-Terrestrial Physics*, *61*, 181-186. https://doi.org/10.1016/S1364-6826(98)00126-6

Gelaro, R., McCarty, W., Suárez, M. J., Todling, R., Molod, A, Takacs, L, et al. (2017). The Modern-Era Retrospective Analysis for Research and Applications, Version 2 (MERRA-2). *Journal of Climate*, *30*, 5419-5454. https://doi.org/10.1175/JCLI-D-16-0758.1

Ghil, M., & Mo, K. (1991). Intraseasonal oscillations in the global atmosphere. Part I: Northern Hemisphere and tropics. *Journal of the Atmospheric Sciences*, *48*, 752-779. https://doi.org/10.1175/1520-0469(1991)048<0752:IOITGA>2.0.CO;2

Guharay, A., Batista, P. P., Buriti, R. A., & Schuch, N. J. (2017). Signature of the quasi-27-day oscillation in the MLT and its relation with solar irradiance and convection. *Journal of Atmospheric and Solar-Terrestrial Physics*, *161*, 1-7. https://doi.org/10.1016/j.jastp.2017.06.001

Guharay, A., Batista, P. P., Clemesha, B. R., & Buriti, R. A. (2014). Observations of the intraseasonal oscillations over two Brazilian low latitude stations: A comparative study. *Journal of Atmospheric and Solar-Terrestrial Physics*, *120*, 62-69. https://doi.org/10.1016/j.jastp.2014.08.016

Gutzler, D. S., & Madden, R. A. (1989). Seasonal variations in the spatial structure of intraseasonal tropical wind fluctuations. *Journal of the Atmospheric Sciences*, *46*, 641-660. https://doi.org/10.1175/1520-0469(1989)046<0641:SVITSS>2.0.CO;2

Hendon, H. H., & Salby, M. L. (1994). The life cycle of the Madden-Julian Oscillation. *Journal of the Atmospheric Sciences*, *51*, 2225-2237.

https://doi.org/10.1175/1520-0469(1994)051<2225:TLCOTM>2.0.CO;2

Hocking, W. K., Fuller, B., & Vandepeer, B. (2001). Real-time determination of meteor-related parameters utilizing modern digital technology. *Journal of Atmospheric and Solar-Terrestrial Physics*, *63*, 155-169. https://doi.org/10.1016/S1364-6826(00)00138-3

Hoffmann, C. G., & von Savigny, C. (2019). Indications for a potential synchronization between the phase evolution of the Madden–Julian oscillation and the solar 27-day cycle. *Atmospheric Chemistry and Physics*, *19*, 4235-4256. https://doi.org/10.5194/acp-19-4235-2019

Hood, L. L. (2016). Lagged response of tropical tropospheric temperature to solar ultraviolet variations on intraseasonal time scales. *Geophysical Research Letters*, *43*(8), 4066-4075. https://doi.org/10.1002/2016GL068855

Hsu, P.-C. & Li, T. (2011). Interactions between boreal summer intraseasonal oscillations and synoptic-scale disturbances over the western North Pacific. Part II: Apparent heat and moisture sources and eddy momentum transport. *Journal of Climate*, *24*, 942-961. https://doi.org/10.1175/2010JCLI3834.1

Huang, K. M., Liu, A. Z., Lu, X., Li, Z., Gan, Q., Gong, Y., Huang, C. M., Yi, F., & Zhang, S. D. (2013a). Nonlinear coupling between quasi 2 day wave and tides based on meteor radar observations at Maui. *Journal of Geophysical Research: Atmospheres*, *118*, 10936-10943. https://doi.org/10.1002/jgrd.50872

Huang, K. M., Liu, A. Z., Zhang, S. D., Yi, F., Huang, C. M., Gan, Q., Gong, Y., & Zhang, Y. H. (2013b). A nonlinear interaction event between a 16-day wave and a diurnal tide from meteor radar observations. *Annales Geophysicae*, *31*, 2039-2048. https://doi.org/10.5194/angeo-31-2039-2013

Huang, K. M., Liu, A. Z., Zhang, S. D., Yi, F., Huang, C. M., Gan, Q., Gong, Y., Zhang, Y. H., & Wang, R. (2015). Observational evidence of quasi-27-day oscillation propagating from the lower atmosphere to the mesosphere over 20° N. *Annales Geophysicae*, *33*, 1321-1330. https://doi.org/10.5194/angeo-33-1321-2015

Huang, K. M., Yang, Z. X., Wang, R., Zhang, S. D., Huang, C. M., Yi, F., & Hu, F. (2018). A Statistical study of inertia gravity waves in the lower stratosphere over the Arctic region based on radiosonde observations. *Journal of Geophysical Research: Atmospheres*, *123*, 4958-4976. https://doi.org/10.1029/2017JD027998

Huang, P., Chou, C., & Huang, R. (2011). Seasonal modulation of tropical intraseasonal oscillations on tropical cyclone geneses in the western North Pacific. *Journal of Climate*, *24*, 6339-6352. https://doi.org/10.1175/2011JCLI4200.1

Isoda, F., Tsuda, T., Nakamura, T., Vincent, R. A., Reid, I. M., Achmad, E., Sadewo, A. & Nuryanto, A. (2004). Intraseasonal oscillations of the zonal wind near the mesopause observed with medium-frequency and meteor radars in the tropics. *Journal of Geophysical Research: Atmospheres*, *109*, D21108. https://doi.org/10.1029/2003JD003378

Jiang, X., Li, T., & Wang, B. (2004). Structures and mechanisms of the northward propagating boreal summer intraseasonal oscillation. *Journal of Climate*, *17*, 1022-1039. https://doi.org/10.1175/1520-0442(2004)017<1022:SAMOTN>2.0.CO;2

Karmakar, N., & Krishnamurti, T. N. (2019). Characteristics of northward propagating intraseasonal oscillation in the Indian summer monsoon. *Climate Dynamics*, *52*, 1903-1916. https://doi.org/10.1007/s00382-018-4268-2

Kumar, K., & Jain, A. R. (1994). Latitudinal variations of 30-70 day period waves over the tropical Indian zone. *Journal of Atmospheric and Terrestrial Physics*, *56*, 1135-1145. https://doi.org/10.1016/0021-9169(94)90052-3

Kumar, K. K., Antonita, T. M., Ramkumar, G., Deepa, V., Gurubaran, S., & Rajaram R. (2007). On the tropospheric origin of Mesosphere Lower Thermosphere region intraseasonal wind variability. *Journal of Geophysical Research: Atmospheres*, *112*, D07109. https://doi.org/10.1029/2006JD007962

Laštovička, J. (2006). Forcing of the ionosphere by waves from below. *Journal of Atmospheric and Solar-Terrestrial Physics*, *68*, 479-497. https://doi.org/10.1016/j.jastp.2005.01.018

Lau, K.-M., & Peng, L. (1990). Origin of low frequency (intraseasonal) oscillations in the tropical atmosphere. Part III: Monsoon dynamics. *Journal of the Atmospheric Sciences*, *47*, 1443-1462. https://doi.org/10.1175/1520-0469(1990)047<1443:OOLFOI>2.0.CO;2

Lau, K.-M., & Wu, H.-T. (2010). Characteristics of precipitation, cloud, and latent heating associated with the Madden-Julian oscillation. *Journal of Climate*, *23*, 504-518. https://doi.org/10.1175/2009JCLI2920.1

Lawrence, D. M., & Webster, P. J. (2001). Interannual variations of the intraseasonal oscillation in the south Asian summer monsoon region. *Journal of Climate*, *14*, 2910-2922. https://doi.org/10.1175/1520-0442(2001)014<2910:IVOTIO>2.0.CO;2

Liebmann, B., & Smith, C. A. (1996). Description of a complete (interpolated) outgoing longwave radiation dataset. *Bulletin of the American Meteorological Society*, *77*, 1275-1277.

Lieberman, R. S. (1998). Intraseasonal variability of high-resolution Doppler imager winds in the equatorial mesosphere and lower thermosphere. *Journal of Geophysical Research: Atmospheres*, *103*, 11221-11228. https://doi.org/10.1029/98JD00532

Lindzen, R. S. (1981). Turbulence and stress owing to gravity wave and tidal breakdown. *Journal of Geophysical Research: Oceans*, *86*, 9707-9714. https://doi.org/10.1029/JC086iC10p09707

Liu, A. Z., Lu, X., & Franke, S. J. (2013). Diurnal variation of gravity wave momentum flux and its forcing on the diurnal tide. *Journal of Geophysical Research: Atmospheres*, *118*, 1668-1678.

https://doi.org/10.1029/2012JD018653

Liu, L., Wan, W., Ning, B., Pirog, O. M., & Kurkin, V. I. (2006). Solar activity variations of the ionospheric peak electron density. *Journal of Geophysical Research: Space Physics*, *111*, A08304. https://doi.org/10.1029/2006JA011598

Li, Z., Li, Y., Bonsal, B., Manson, A. H., & Scaff, L. (2018). Combined impacts of ENSO and MJO on the 2015 growing season drought on the Canadian Prairies. *Hydrology and Earth System Sciences*, 22, 5057-5067. https://doi.org/10.5194/hess-22-5057-2018

Lu, X., Liu, A. Z., Oberheide, J., Wu, Q., Li, T., Li, Z., Swenson, G. R., & Franke, S. J. (2011). Seasonal variability of the diurnal tide in the mesosphere and lower thermosphere over Maui, Hawaii (20.7˚N, 156.3˚W). *Journal of Geophysical Research*, *116*, D17103. https://doi.org/10.1029/2011JD015599

Luo, Y., Manson, A. H., Meek, C. E., Igarashi, K., & Jacobi, C. (2001). Extra long period (20-40 day) oscillations in the mesospheric and lower thermospheric winds: observations in Canada, Europe and Japan, and considerations of possible solar influences. *Journal of Atmospheric and Solar-Terrestrial Physics*, *63*, 835-852. https://doi.org/10.1016/S1364-6826(00)00206-6

Madden, R. A. (1986). Seasonal variations of the 40-50 day oscillation in the tropics. *Journal of the Atmospheric Sciences*, *43*, 3138-3158. https://doi.org/10.1175/1520-0469(1986)043<3138:SVOTDO>2.0.CO;2

Madden, R. A., & Julian, P. R. (1971). Detection of a 40-50 day oscillation in the zonal wind in the tropical Pacific, *Journal of the Atmospheric Sciences*, *28*, 702-708. https://doi.org/10.1175/1520-0469(1971)028<0702:DOADOI>2.0.CO;2

Madden, R. A., & Julian, P. R. (1972). Description of global-scale circulation cells in the tropics with a 40-50 day period. *Journal of the Atmospheric Sciences*, *29*, 1109-1123.

https://doi.org/10.1175/1520-0469(1972)029<1109:DOGSCC>2.0.CO;2

Madden, R. A., & Julian, P. R. (1994). Observations of the 40-50-day tropical oscillation-A review. *Monthly Weather Review*, *122*, 814-837. https://doi.org/10.1175/1520-0493(1994)122<0814:OOTDTO>2.0.CO;2

Ma, R., Xu, J., Wang, W., & Lei, J. (2012). The effect of ~27 day solar rotation on ionospheric F_2 region peak densities (N_mF_2). *Journal of Geophysical Research: Space Physics*, *117*, A03303, https://doi.org/10.1029/2011JA017190

Mikhailov, A. V., Depueva, A. Kh., & Leschinskaya, T. Yu. (2004). Morphology of quiet time F2-layer disturbances: High to lower latitudes. *International Journal of Geomagnetism and Aeronomy*, *5*, 1-14, GI1006. https://doi.10.1029/2003GI000058

Min, K., Park, J., Kim, H., Kim, V., Kil, H., Lee, J., Rentz, S., Lühr, H., & Paxton, L. (2009). The 27-day modulation of the low-latitude ionosphere during a solar maximum. *Journal of Geophysical Research: Space Physics*, *114*, A04317. https://doi.org/10.1029/2008JA013881

Moss, A. C., Wright, C. J., & Mitchell, N. J. (2016). Does the Madden-Julian Oscillation modulate stratospheric gravity waves? *Geophysical Research Letters*, *43*, 3973-3981. https://doi.org/10.1002/2016GL068498

Nagpal, O. P., Dhaka, S. K., & Srivastav, S. K. (1994). Wave characteristics in the troposphere and stratosphere over the Indian tropics during the DYANA period. *Journal of Atmospheric and Terrestrial Physics*, *56*, 1117-1133. https://doi.org/10.1016/0021-9169(94)90051-5

Niranjankumar, K., Ramkumar, T. K., & Krishnaiah, M. (2011). Vertical and lateral propagation characteristics of intraseasonal oscillation from the tropical lower troposphere to upper mesosphere. *Journal of Geophysical Research: Atmospheres*, *116*, D21112. https://doi.org/10.1029/2010JD015283

Pancheva, D., Mitchell, N., Clark, R. R., Drobjeva, J., & Lastovicka, J. (2002). Variability in the maximum height of the ionospheric F2-layer over Millstone Hill (September 1998-March 2000); influence from below and above. *Annales Geophysicae*, *20*, 1807-1819. https://doi.org/10.5194/angeo-20-1807-2002

Pancheva, D., Mitchell, N. J., Younger, P. T., & Muller, H. G. (2003) Intra-seasonal oscillations observed in the MLT region above UK (52°N, 2°W) and ESRANGE (68°N, 21°E). *Geophysical Research Letters*, *30*, 2084. https://doi.org/10.1029/2003GL017809

Pancheva, D., Schminder, R., & Laštovička, J. (1991). 27-day fluctuations in the ionospheric D-region. *Journal of Atmospheric and Terrestrial Physics*, *53*, 1145-1150. https://doi.org/10.1016/0021-9169(91)90064-E

Pancheva, D. V., Mukhtarov, P. J., Shepherd, M. G., Mitchell, N. J., Fritts, D. C., Riggin, D. M., et al. (2006). Two-day wave coupling of the low-latitude atmosphere-ionosphere system. *Journal of Geophysical Research: Space Physics*, *111*, A07313. https://doi.org/10.1029/2005JA011562

Rao, R. K., Gurubaran, S., Sathishkumar, S., Sridharan, S., Nakamura, T., Tsuda, T., Takahashi H., Batista, P. P., Clemesha, B. R., Buriti, R. A., Pancheva, D. V., & Mitchell, N. J. (2009). Longitudinal variability in intraseasonal oscillation in the tropical mesosphere and lower thermosphere region. *Journal of Geophysical Research: Atmospheres*, *114*, D19110. https://doi.org/10.1029/2009JD011811

Reed, R. J., Campbell, W. J., Rasmussen, L. A., & Rogers, D. G. (1961). Evidence of a downward-propagating, annual wind reversal in the equatorial stratosphere. *Journal of Geophysical Research*, *66*, 813-818. https://doi.org/10.1029/JZ066i003p00813

Reinisch, B. W., Galkin, I. A., Khmyrov, G., Kozlov, A., & Kitrosser, D. F. (2004). Automated collection and dissemination of ionospheric data from the digisonde network. *Advances in Radio*

Science, *2*, 241-247. https://doi.org/10.5194/ars-2-241-2004

Ren, D., Lei, J., Wang, W., Burns, A., Luan, X., & Dou, X. (2018). Does the peak response of the ionospheric F_2 region plasma lag the peak of 27-day solar flux variation by multiple days? *Journal of Geophysical Research: Space Physics*, *123*, 7906-7916. https://doi.org/10.1029/2018JA025835

Richards, P. G. (2001). Seasonal and solar cycle variations of the ionospheric peak electron density: Comparison of measurement and models. *Journal of Geophysical Research: Space Physics*, *106*, 12803-12819. https://doi.org/10.1029/2000JA000365

Rich, F. J., Sultan, P. J., & Burke, W. J. (2003). The 27-day variations of plasma densities and temperatures in the topside ionosphere. *Journal of Geophysical Research: Space Physics*, *108*, 1297. https://doi.org/10.1029/2002JA009731

Rishbeth, H., & Mendillo, M. (2001). Patterns of F2-layer variability. *Journal of Atmospheric and Solar-Terrestrial Physics*, *63*, 1661-1680. https://doi.org/10.1016/S1364-6826(01)00036-0

Salby, M. L., Garcia, R. R., & Hendon, H. H. (1994). Planetary-scale circulations in the presence of climatological and wave-induced heating. *Journal of the Atmospheric Sciences*, *51*, 2344-2367. https://doi.org/10.1175/1520-0469(1994)051<2344:PSCITP>2.0.CO;2

Scargle, J. D. (1982). Studies in astronomical time series analysis. II. Statistical aspects of spectral analysis of unevenly spaced data. *The Astrophysical Journal*, *263*, 835-853.

Schanz, A., Hocke, K., & Kämpfer, N. (2016). On forced and free atmospheric oscillations near the 27-day periodicity. *Earth, Planets and Space*, 68:97. https://doi.org/10.1186/s40623-016-0460-y

Solomon, S. C., Qian, L., & Mannucci, A. J. (2018). Ionospheric electron content during solar cycle 23. *Journal of Geophysical Research: Space Physics*, *123*, 5223-5231. https://doi.org/10.1029/2018JA025464

Sukhodolov, T., Rozanov, E., Ball, W. T., Peter, T., & Schmutz, W. (2017). Modeling of the middle atmosphere response to 27-day solar irradiance variability. *Journal of Atmospheric and Solar-Terrestrial Physics*, *152*, 50-61. http://dx.doi.org/10.1016/j.jastp.2016.12.004

Thiéblemont, R., Bekki, S., Marchand, M., Bossay, S., Schmidt, H., Meftah, M., & Hauchecorne A. (2018). Nighttime mesospheric/lower thermospheric tropical ozone response to the 27-day solar rotational cycle: ENVISAT-GOMOS satellite observations versus HAMMONIA idealized chemistry-climate model simulations. *Journal of Geophysical Research: Atmospheres*, *123*, 8883-8896. https://doi.org/10.1029/2017JD027789

Tsuchiya, C., Sato, K., Alexander, M. J., & Hoffmann, L. (2016). MJO-related intraseasonal variation of gravity waves in the Southern Hemisphere tropical stratosphere revealed by high-resolution AIRS observations. *Journal of Geophysical Research: Atmospheres*, *121*, 7641-7651. https://doi.org/10.1002/2015JD024463

Vincent, R. A., & Alexander, M. J. (2000). Gravity waves in the tropical lower stratosphere: An observational study of seasonal and interannual variability. *Journal of Geophysical Research: Atmospheres*, *105*, 17971-17982. https://doi.org/10.1029/2000JD900196

Wang, B., & Xie, X. (1996). Low-frequency equatorial waves in vertically sheared zonal flow. Part I: Stable waves. *Journal of the Atmospheric Sciences*, *53*, 449-467. https://doi.org/10.1175/1520-0469(1996)053<0449:LFEWIV>2.0.CO;2

Wang, B., & Xie, X. (1997). A model for the boreal summer intraseasonal oscillation. *Journal of the Atmospheric Sciences*, *54*, 72-86. https://doi.org/10.1175/1520-0469(1997)054<0072:AMFTBS>2.0.CO;2

Xu, J., Wang, W., Lei, J., Sutton, E. K., & Chen, G. (2011). The effect of periodic variations of thermospheric density on CHAMP and GRACE orbits. *Journal of Geophysical Research: Space Physics*, *116*, A02315. https://doi.org/10.1029/2010JA015995

Yang, L., Du, Y., Wang, D., Wang, C., & Wang, X. (2015). Impact of intraseasonal oscillation on the tropical cyclone track in the South China Sea. *Climate Dynamics*, *44*, 1505-1519. https://doi.org/10.1007/s00382-014-2180-y

Zhang, C. (2005). Madden-Julian Oscillation. *Reviews of Geophysics*, *43*, RG2003. https://doi.org/10.1029/2004RG000158

Zhang, S. D., & Yi, F. (2007). Latitudinal and seasonal variations of inertial gravity wave activity in the lower atmosphere over central China. *Journal of Geophysical Research: Atmospheres*, *112*, D05109. https://doi.org/10.1029/2006JD007487

Zhang, S. D., Yi, F., Huang, C. M., & Huang, K. M. (2012). High vertical resolution analyses of gravity waves and turbulence at a midlatitude station. *Journal of Geophysical Research: Atmospheres*, *117*, D02103. https://doi.org/10.1029/2011JD016587

Zhou, W., & Chan, J. C. L. (2005). Intraseasonal oscillations and the South China Sea summer monsoon onset. *International Journal of Climatology*, *25*, 1585-1609. https://doi.org/10.1002/joc.1209

Ziemke, J. R., & Stanford, J. L. (1991). One-to-two month oscillations: observed high-latitude tropospheric and stratospheric response to tropical forcing. *Journal of the Atmospheric Sciences*, *48*, 1336-1347. https://doi.org/10.1175/1520-0469(1991)048<1336:OTTMOO>2.0.CO;2

Caption:

Figure 1. Daily mean (a) zonal and (b) meridional winds from Maui meteor radar observation for 81 days from 12 August to 31 October 2006.

Figure 2. Lomb-Scargle spectra of (a) zonal and (b) meridional winds observed by Maui meteor radar. The dashed vertical line corresponds to a period of 27 days.

Figure 3. (a) Amplitude and (b) phase of quasi 27-day oscillation in zonal wind from Maui meteor radar observation. The asterisk denotes the value derived from the sinusoidal wave fitting, and the dashed line in Panel (b) denotes the linearly fitted phase.

Figure 4. Wavelet spectra of (a) ionospheric hmF2 in Kwajalein and (b) zonal wind at 100 km in Maui.

Figure 5. Lomb-Scargle spectrum of zonal wind from radiosonde observations in (a) Hilo, (b) Kauai and (c) Pago Pago. The dashed vertical line corresponds to a period of 27 days.

Figure 6. Lomb-Scargle spectrum of zonal wind over Maui obtained from MERRA-2 reanalysis data. The dashed vertical line corresponds to a period of 27 days.

Figure 7. Latitudinal evolutions of fitted amplitude and phase in zonal wind at (a) 0.48 hPa and (b) 176.93 hPa levels from MERRA-2 reanalysis data. The asterisk denotes the fitted value.

Figure 8. Lomb-Scargle spectra of daily mean GW energies at (a, c) 1-9 km and (b, d) 20-28 km derived from radiosonde observations. Panels (a, b) represent the spectra of GW energy averaged between Hilo and Kauai, and Panels (c, d) represent the spectra of averaged GW energy in Pago Pago. The dashed vertical line corresponds to a period of 27 days.

Figure 9. Wavelet spectrum of OLR at (20°N, 157.5°W) and (15°S, 170°W), close to Maui and Pago Pago, respectively.

Figure 10. Lomb-Scargle spectrum of specific humidity derived from (a) radiosonde observation and (a) reanalysis data over Pago Pago. The dashed vertical lines correspond to a period of 27 days.

Figure 11. Wavelet spectra of (a) F10.7 and (b) Kp index.

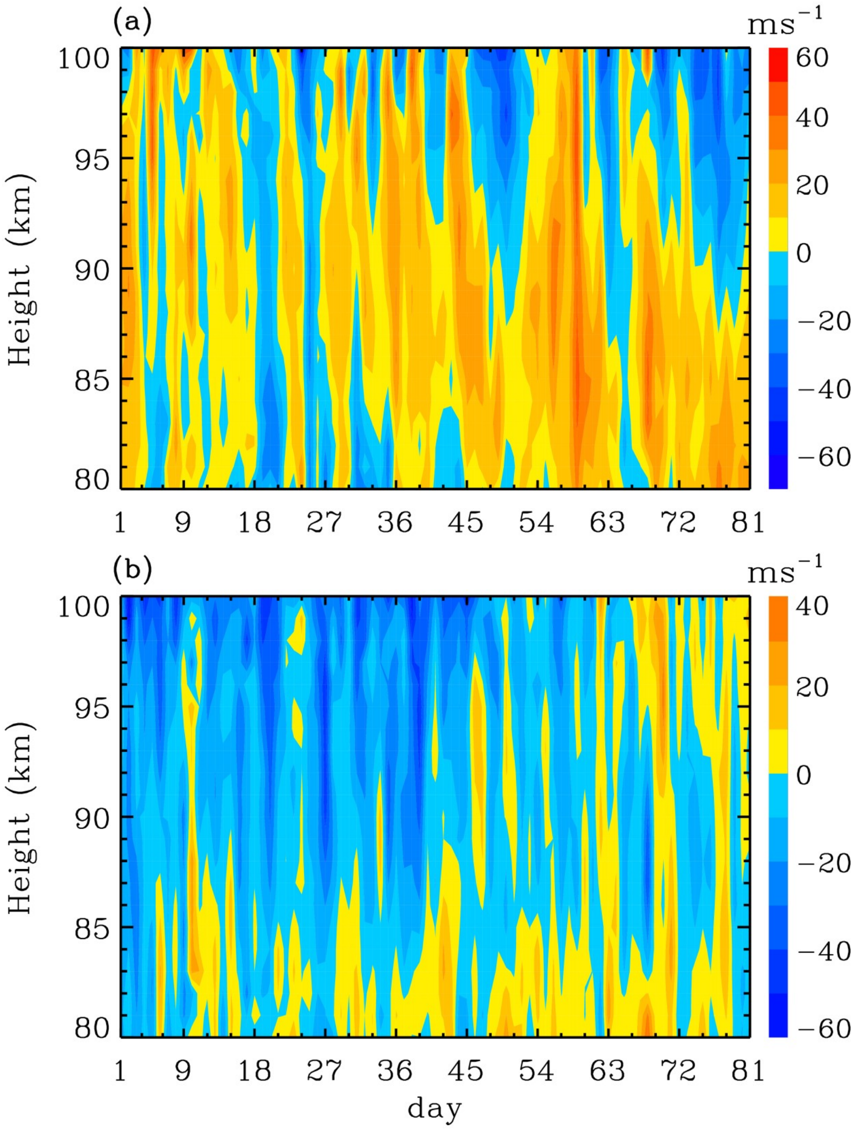

Figure 1. Daily mean (a) zonal and (b) meridional winds from Maui meteor radar observation for 81 days from 12 August to 31 October 2006.

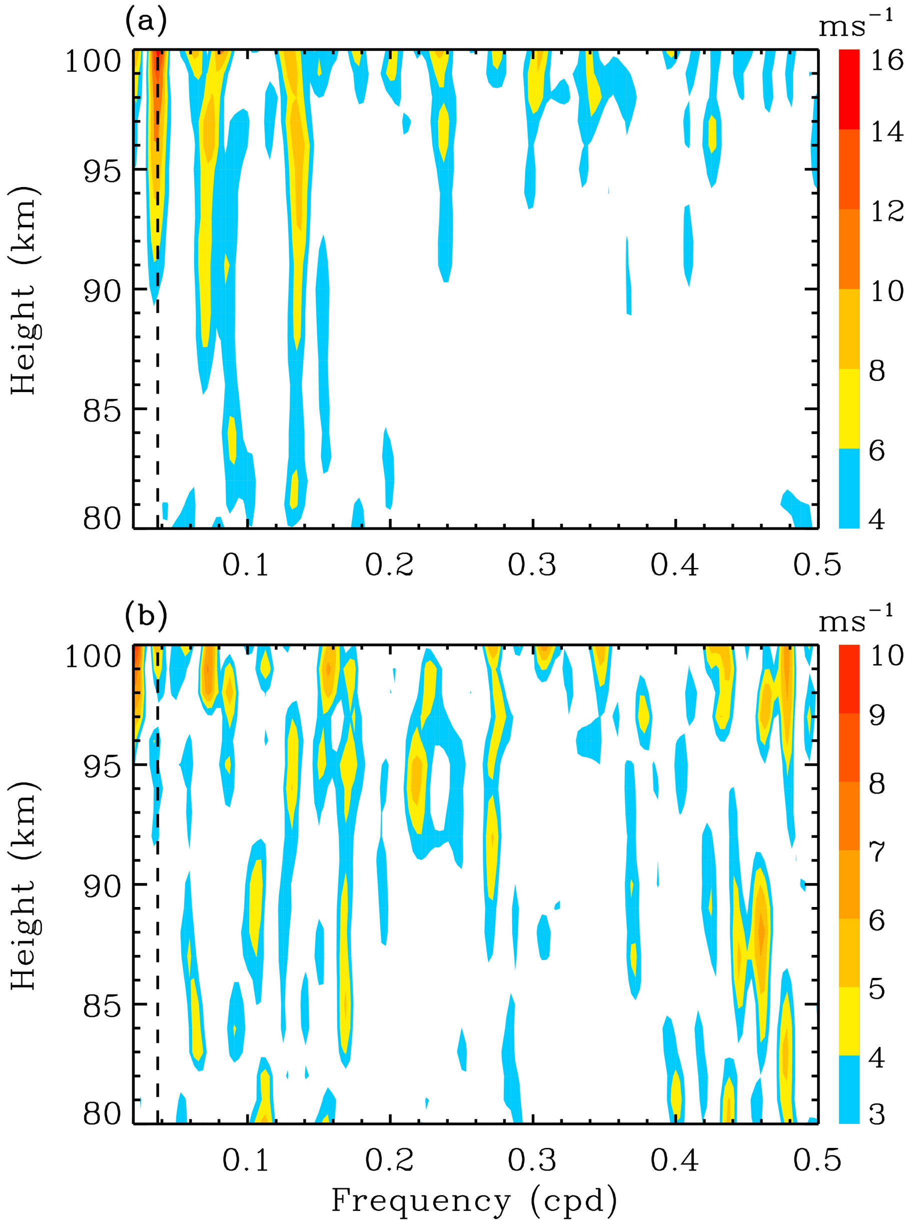

Figure 2. Lomb-Scargle spectra of (a) zonal and (b) meridional winds observed by Maui meteor radar. The dashed vertical line corresponds to a period of 27 days.

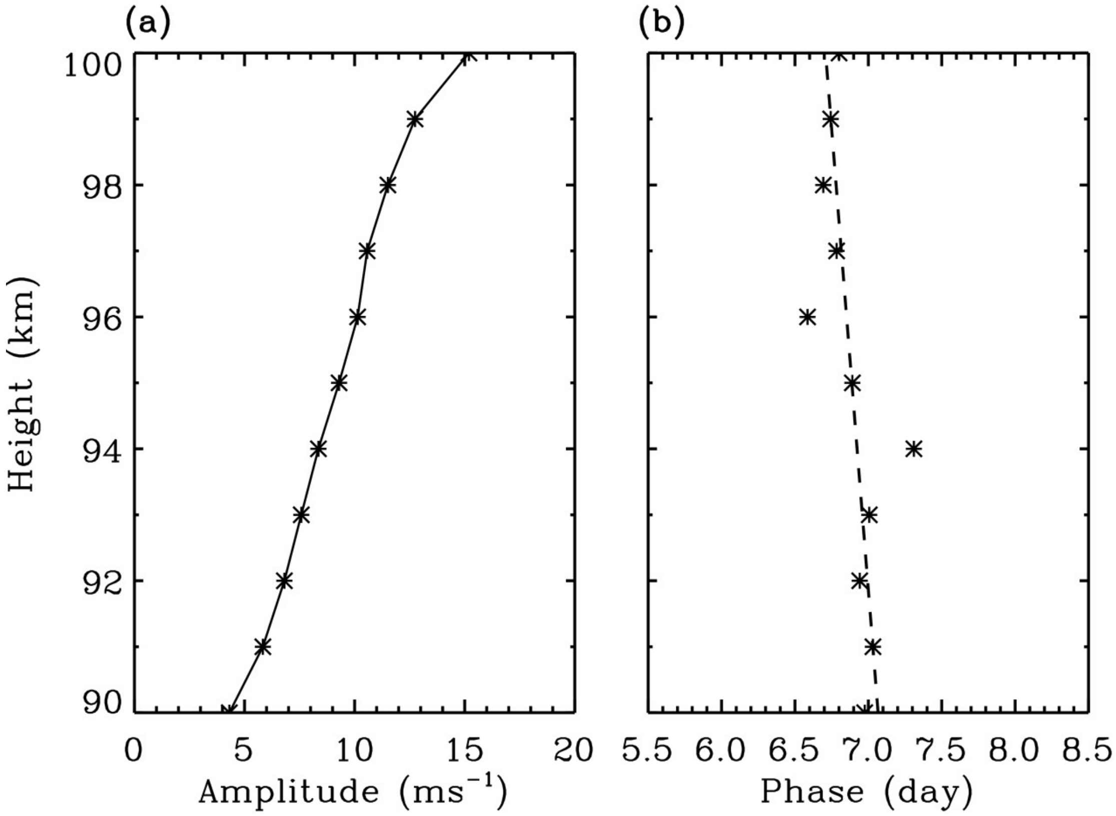

Figure 3. (a) Amplitude and (b) phase of quasi 27-day oscillation in zonal wind from Maui meteor radar observation. The asterisk denotes the value derived from the sinusoidal wave fitting, and the dashed line in Panel (b) denotes the linearly fitted phase.

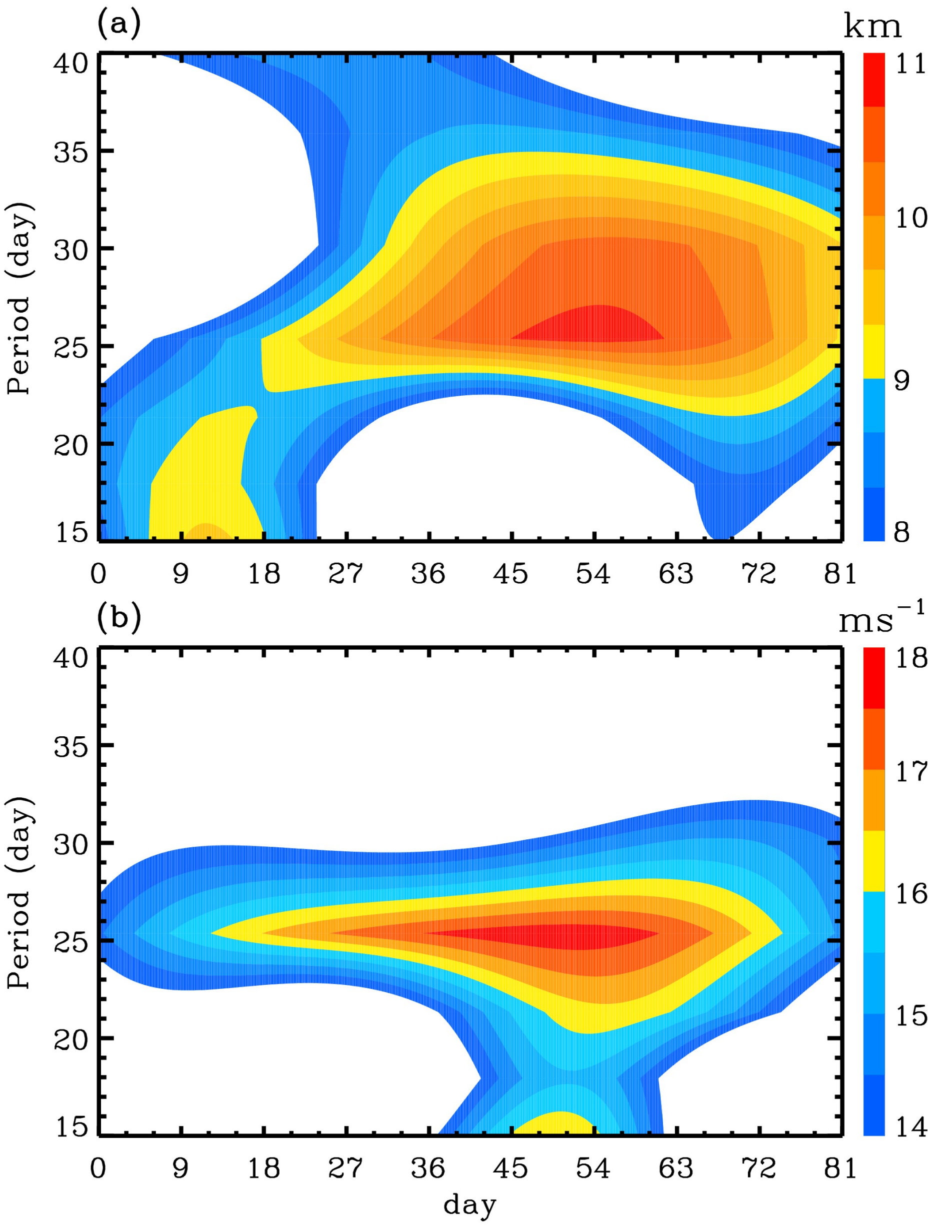

Figure 4. Wavelet spectra of (a) ionospheric hmF2 in Kwajalein and (b) zonal wind at 100 km in Maui.

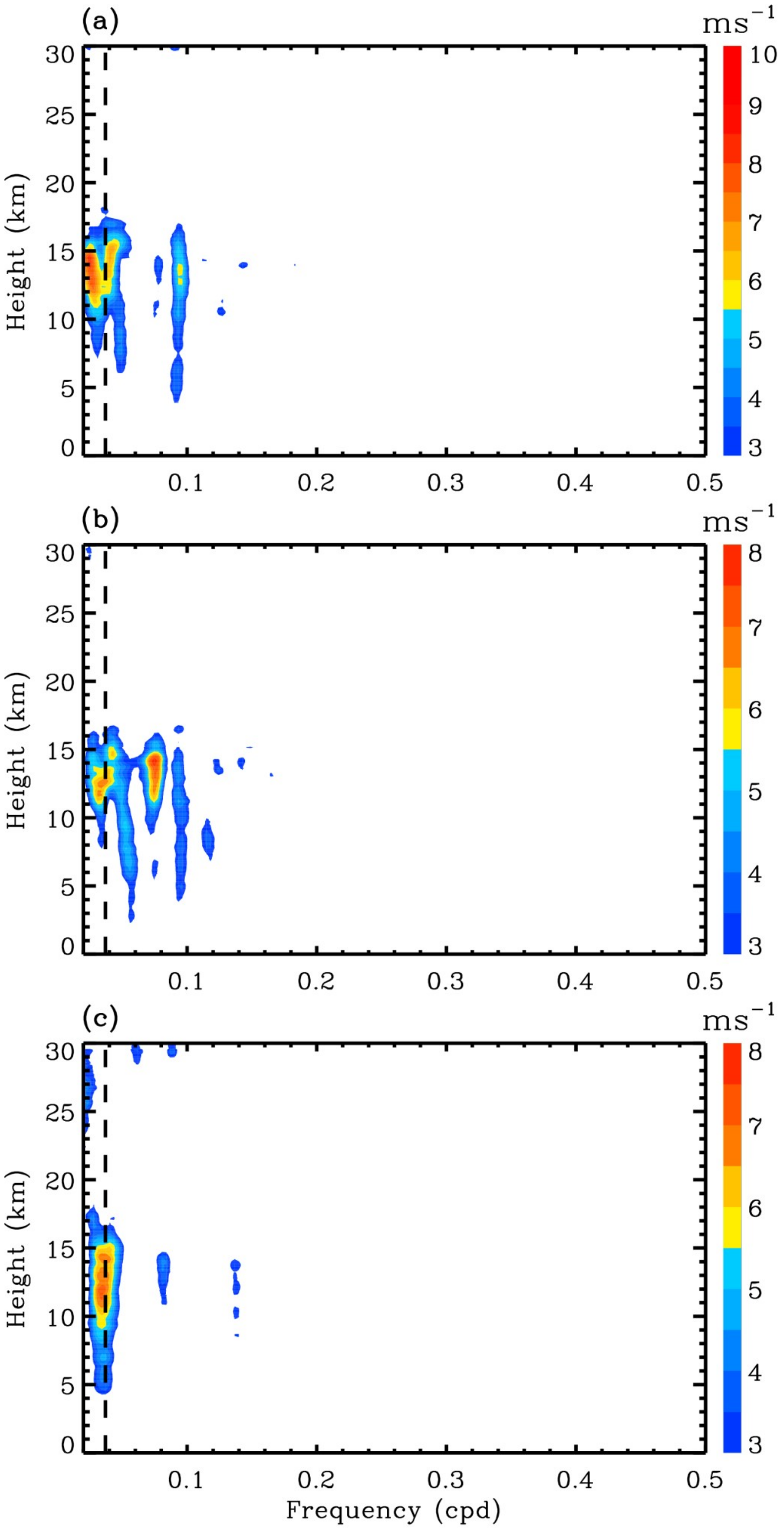

Figure 5. Lomb-Scargle spectrum of zonal wind from radiosonde observations in (a) Hilo, (b) Kauai and (c) Pago Pago. The dashed vertical line corresponds to a period of 27 days.

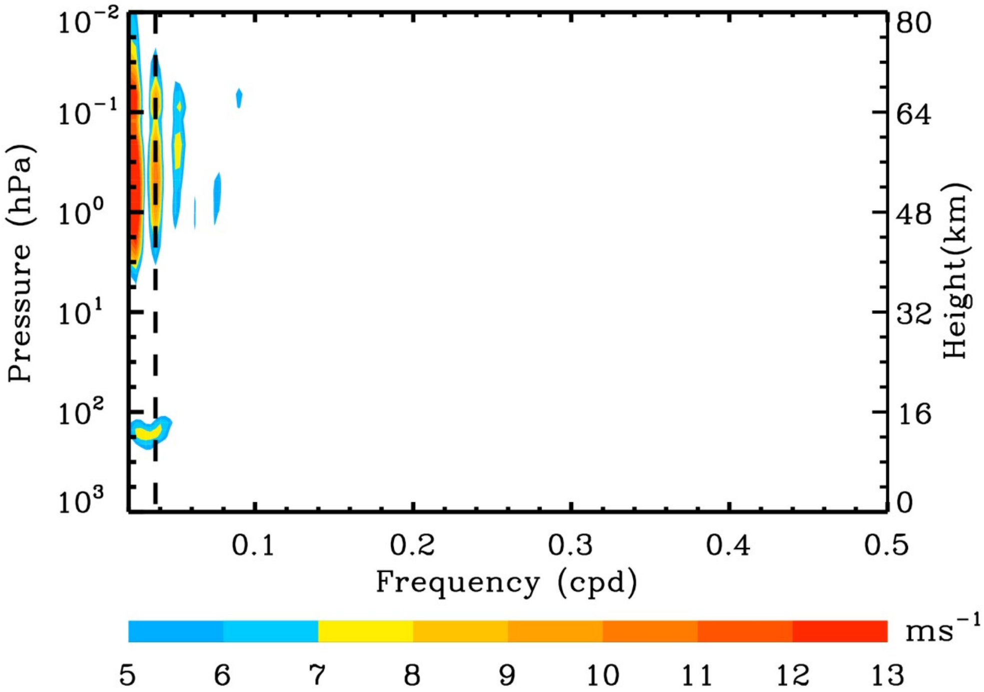

Figure 6. Lomb-Scargle spectrum of zonal wind over Maui obtained from MERRA-2 reanalysis data. The dashed vertical line corresponds to a period of 27 days.

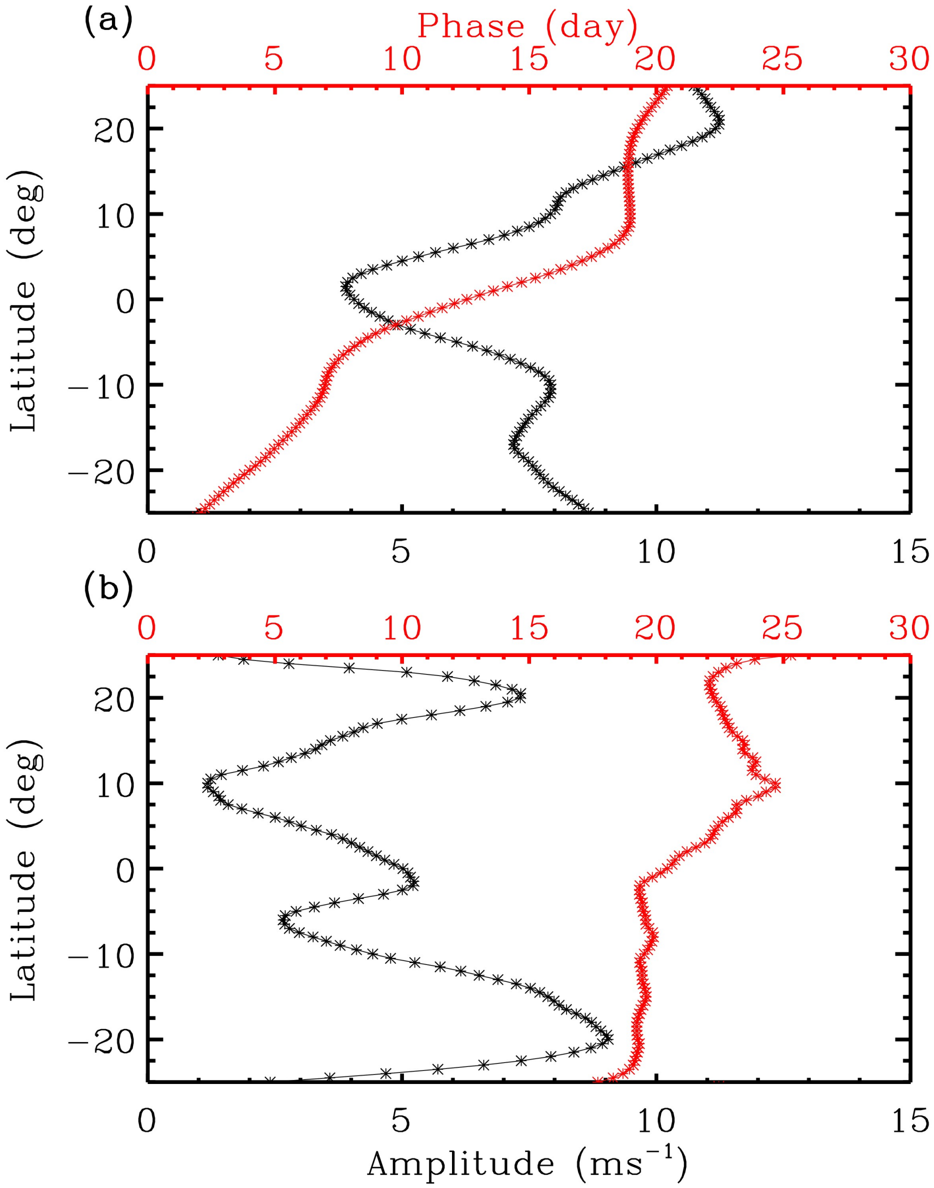

Figure 7. Latitudinal evolutions of fitted amplitude and phase in zonal wind at (a) 0.48 hPa and (b) 176.93 hPa levels from MERRA-2 reanalysis data. The asterisk denotes the fitted value.

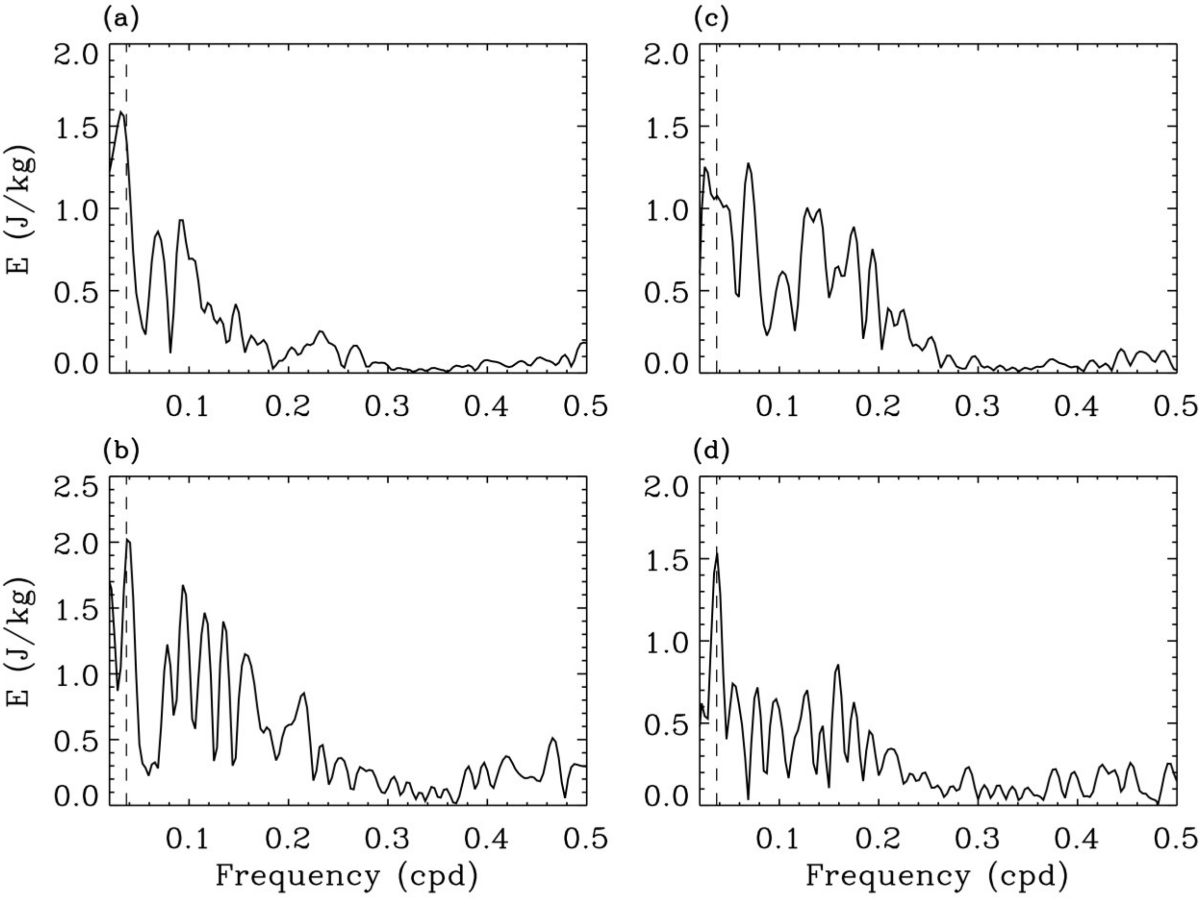

Figure 8. Lomb-Scargle spectra of daily mean GW energies at (a, c) 1-9 km and (b, d) 20-28 km derived from radiosonde observations. Panels (a, b) represent the spectra of GW energy averaged between Hilo and Kauai, and Panels (c, d) represent the spectra of averaged GW energy in Pago Pago. The dashed vertical line corresponds to a period of 27 days.

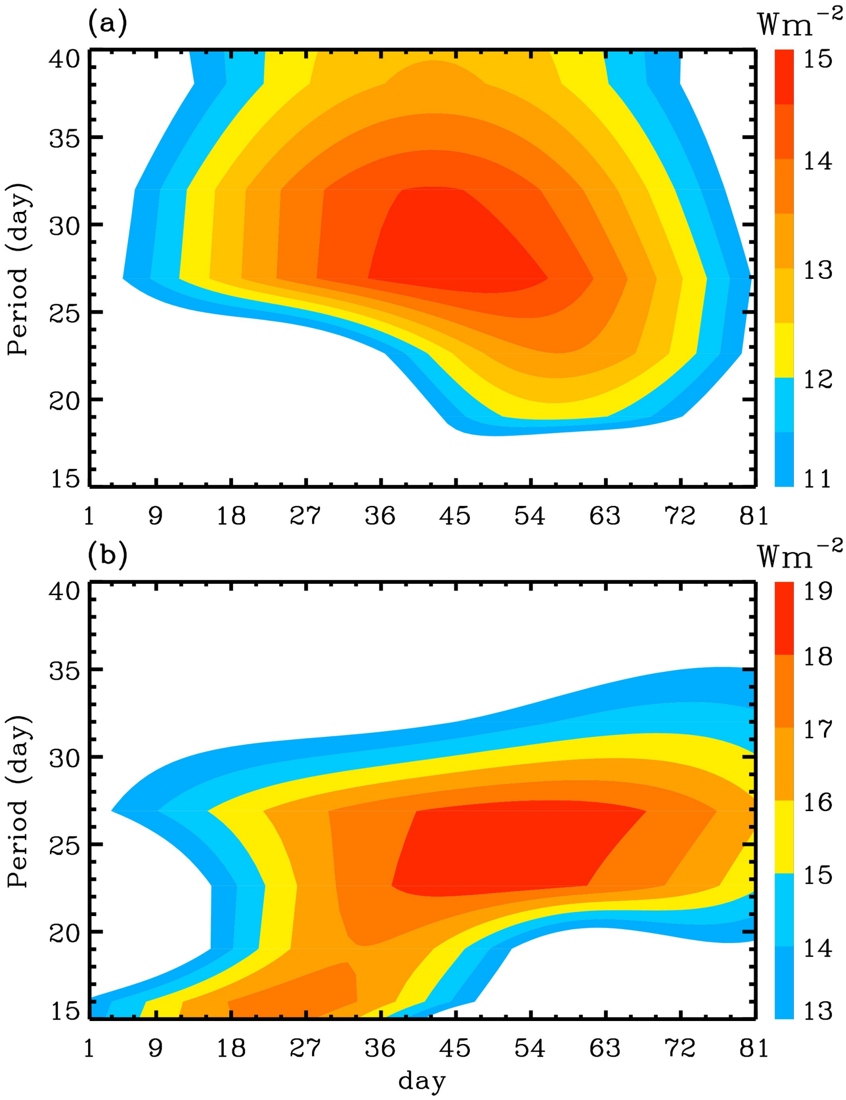

Figure 9. Wavelet spectrum of OLR at (20°N, 157.5°W) and (15°S, 170°W), close to Maui and Pago Pago, respectively.

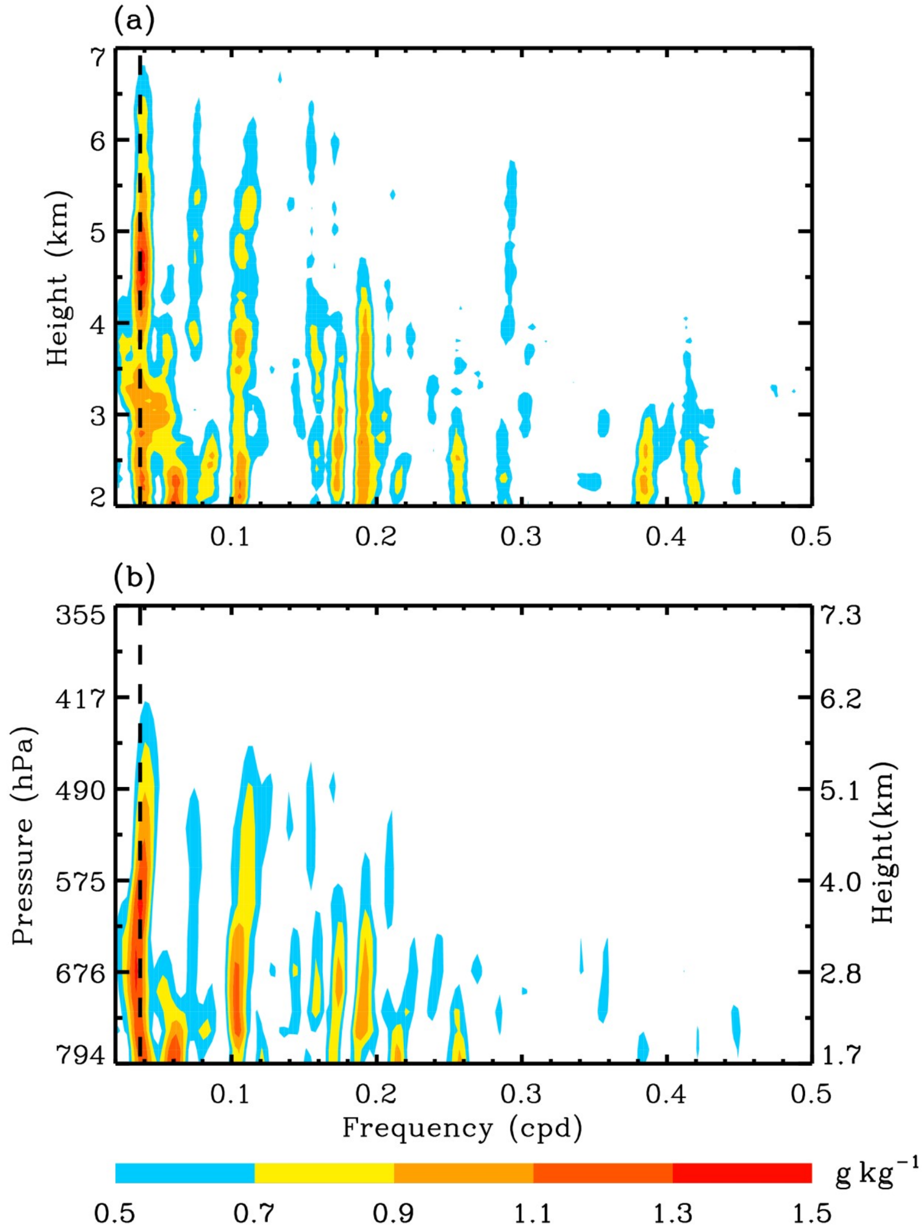

Figure 10. Lomb-Scargle spectrum of specific humidity derived from (a) radiosonde observation and (a) reanalysis data over Pago Pago. The dashed vertical lines correspond to a period of 27 days.

805

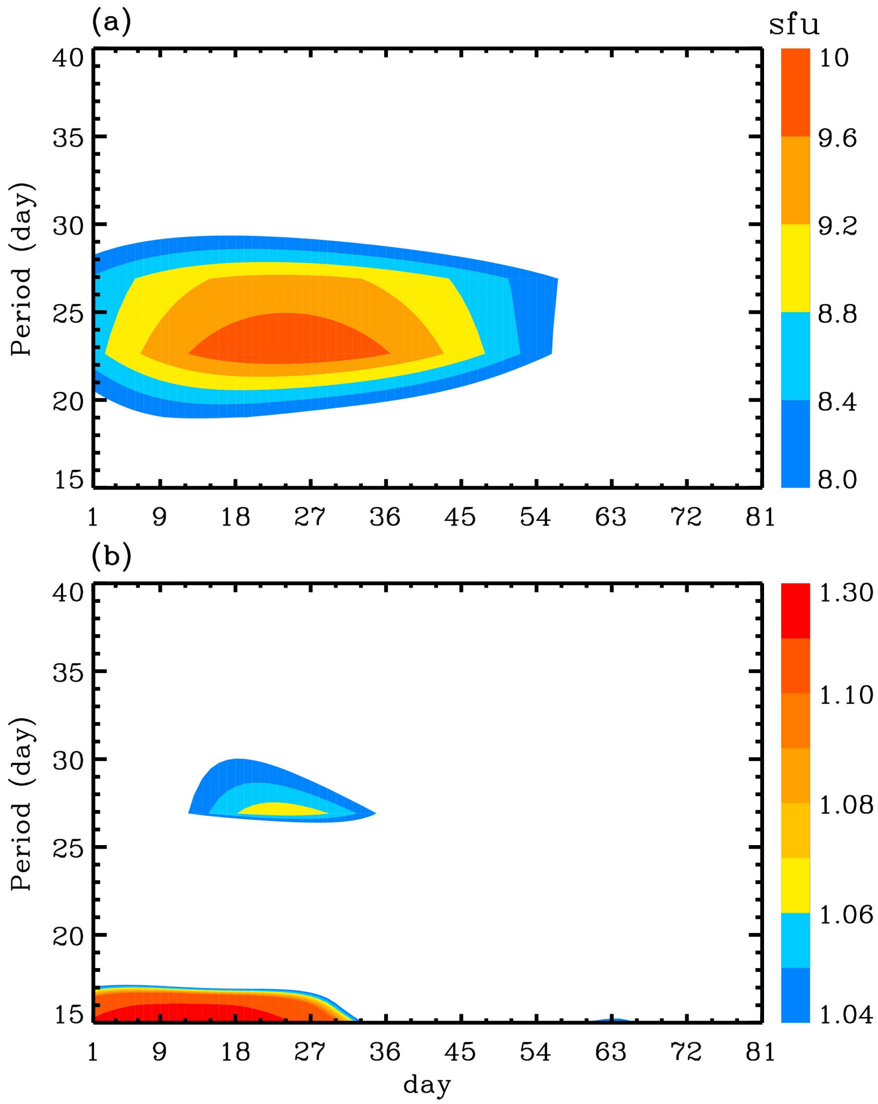

806 **Figure 11.** Wavelet spectra of (a) F10.7 and (b) Kp index.